Am J Cancer Res 2026;16(8):3644-3659
www.ajcr.us /ISSN:2156-6976/ajcr0170738

Original Article

Transcriptional activation of ALOX5 by c-Myc drives malignant progression and M2 macrophage polarization in clear cell renal cell carcinoma

Changjie Ren[1,2*], Yijun Tian[1,2*], Xinran Zhang[1*], Denglong Wu[2], Weidong Zhou[2], Xue Zhang[1]

[1]*Shanghai Health Commission Key Lab of Artificial Intelligence (AI)-Based Management of Inflammation and Chronic Diseases, Sino-French Cooperative Central Lab, Shanghai Pudong Gongli Hospital, Shanghai 200135, China;* [2]*Department of Urology, Tongji Hospital, School of Medicine, Tongji University, Shanghai 200065, China.* [*]*Equal contributors.*

Received December 14, 2025; Accepted July 31, 2026; Epub August 15, 2026; Published August 30, 2026

Abstract: Clear cell renal cell carcinoma (ccRCC) is an aggressive malignancy with poor prognosis, but the molecular mechanisms linking oncogenic signaling to macrophage polarization remain unclear. In this study, we identify arachidonate 5-lipoxygenase (ALOX5) as an oncogenic factor in ccRCC. Multi-omics analyses and clinical validation show that ALOX5 is up-regulated in ccRCC tissues and its high expression is associated with advanced tumor stage and poor survival. Functional assessments reveal that silencing ALOX5 in ccRCC cells inhibits cell proliferation, migration, invasion, and epithelial-to-mesenchymal transition (EMT) *in vitro*, and suppresses tumor progression *in vivo*. Notably, ALOX5 expression in ccRCC cells is positively correlated with the polarization of infiltrating macrophages into the M2 phenotype, and the accumulation of this portion of M2-polarized tumor-associated macrophages (TAMs) in the tumor microenvironment. ALOX5 knockdown reduces macrophage migration and M2 marker expression. Mechanistically, c-Myc directly binds to the ALOX5 promoter and activates its transcription. Restoration of ALOX5 in c-Myc-silenced cells partially rescues the malignant phenotype and M2 polarization, confirming a functional c-Myc-ALOX5 axis. Collectively, our findings suggest that the c-Myc-ALOX5 pathway promotes ccRCC progression by enhancing tumor cell aggressiveness and M2 macrophage polarization, offering a potential therapeutic target for immune microenvironment modulation in renal cancer.

Keywords: ccRCC, ALOX5, c-Myc, TAMs, TIME

Introduction

ccRCC is the predominant and highly invasive form of kidney cancer, representing more than 70% of all renal cancer diagnoses [1, 2]. Although combination strategies utilizing immune checkpoint inhibitors and targeted therapies can prolong survival in some patients, a significant proportion of those with advanced-stage disease still develop drug resistance and experience recurrence, resulting in a 5-year overall survival rate of under 15% [3, 4].

The tumor immune microenvironment (TIME) significantly drives ccRCC progression. Within this TIME, M2-polarized tumor-associated macrophages (TAMs) work together to enhance VEGF-driven angiogenesis by releasing immunosuppressive cytokines like IL-10 and TGF-β [5]. Collectively, this establishes a microenvironment conducive to tumor immune evasion and metastasis, which is strongly linked to adverse clinical outcomes in patients [6-8].

ALOX5 (arachidonate 5-lipoxygenase) is a crucial enzyme in the lipoxygenase (LOX) family that oxygenates arachidonic acid and other polyunsaturated fatty acids to generate bioactive lipid mediators [9-11]. Prior studies show that ALOX5 is aberrantly activated in breast, pancreatic, ovarian, bladder, and glioma, where it facilitates tumor cell growth, migration, and immune escape [12-16]. Although ALOX5 has been confirmed to promote tumorigenesis in intrahepatic cholangiocarcinoma [17], the upstream molecular drivers governing TAM recruit-

https://doi.org/10.62347/CRGB4288

ment and their preferential M2 polarization in ccRCC remain largely unelucidated. Moreover, its expression pattern, functional role, and regulatory mechanisms in ccRCC have not been systematically characterized.

The oncogene c-Myc serves as a key transcription regulator, often misregulated in various cancers, amongst them ccRCC [18-20]. It regulates multiple cellular programs, such as proliferation, metabolism, and apoptosis, and recent studies indicate that it also shapes the tumor immune microenvironment [21-24]. Given its broad regulatory capacity, we hypothesized that c-Myc may transcriptionally regulate ALOX5 and other key oncogenic effectors in ccRCC.

This study proposes the c-Myc/ALOX5 axis as a key promoter of clear cell renal cell carcinoma (ccRCC) progression. Elevated ALOX5 expression and its negative correlation with prognosis were observed in ccRCC. Functional assessments elucidated that ALOX5 expression promotes the malignant phenotype of ccRCC cells both *in vitro* and *in vivo*. Furthermore, we revealed a novel mechanism whereby high-ALOX5-expression ccRCC cells orchestrate the recruitment and M2 polarization of tumor-associated macrophages (TAMs), which contributed to the establishment of a pro-tumorigenic microenvironment. Our findings establish the c-Myc/ALOX5 axis as a potential therapeutic target in ccRCC.

Materials and methods

Bioinformatics analysis

The TCGA-KIRC (Kidney Renal Clear Cell Carcinoma) dataset is a publicly available genomic resource generated by The Cancer Genome Atlas (TCGA) program, comprising RNA-sequencing data and corresponding clinical annotations from ccRCC patients. Transcriptomic profiles quantified by the STAR pipeline and expressed as transcripts per million (TPM), together with corresponding clinical annotations, were downloaded from the GDC data portal (https://portal.gdc.cancer.gov) and log2(TPM + 1)-transformed prior to analysis. The original cohort comprises 613 samples in total, including 541 primary tumor samples (TCGA sample type code: 01) and 72 adjacent normal tissue samples (TCGA sample type code: 11). For paired differential expression analysis, 72 tumor-normal matched pairs were retained, comprising patients for whom both primary tumor and matched adjacent normal tissue samples were simultaneously available. For survival analyses, the optimal cutoff value of ALOX5 expression was determined separately for each endpoint using maximally selected rank statistics (the surv_cutpoint function of the survminer package), and patients were stratified into high- and low-expression groups accordingly. Overall survival and disease-specific survival were then compared between the two groups using Kaplan-Meier estimators and log-rank tests, implemented with the survival and survminer packages.

To validate ALOX5 expression in independent ccRCC cohorts, four gene expression datasets were retrieved from the Gene Expression Omnibus (GEO) database. Datasets were selected according to the following criteria: (1) the study profiled ccRCC tumor tissues together with paired or unpaired normal/adjacent non-tumor renal tissues, permitting tumor-versus-normal comparison; (2) genome-wide mRNA expression data were publicly available; and (3) sample annotation was sufficient to unambiguously classify each sample as tumor or normal. Accordingly, GSE46699 [25] (65 ccRCC and 61 patient-matched normal kidney tissues), GSE40435 [26] (101 paired ccRCC and adjacent non-tumor tissues), GSE53757 [27] (72 ccRCC and 72 matched normal tissues), and GSE15641 [28] (ccRCC and normal kidney tissues selected from the original cohort) were included. As all four datasets were generated on microarray platforms, differential expression analyses were performed using the *limma* package. The two data types were analyzed using different approaches according to their structure: ALOX5 expression in the TCGA-KIRC cohort was directly compared between groups using the non-parametric Wilcoxon rank-sum test on log2(TPM + 1) values, whereas genome-wide differential expression in the intensity-based GEO microarray datasets was assessed using the linear-modeling framework implemented in limma. The immune cell composition based on the datasets acquired from TCGA was inferred using the CIBERSORT algorithm [29]. The association between ALOX5 expression and classic M2 macrophage markers (CD163 and CD206) was evaluated using Pearson's correlation analysis, implemented via the *cor.test* function in R.

Correlation strength was assessed by the coefficient (r) along with the corresponding *P*-value. ALOX5 protein levels in ccRCC were analyzed via the CPTAC module of UALCAN [30] (http://ualcan.path.uab.edu). Tumor and normal tissues were compared and visualized in R; significance was tested by t-test with Benjamini-Hochberg correction.

To identify potential transcription factors (TFs) regulating ALOX5, multiple authoritative databases were systematically queried and cross-validated, including KnockTF [31] (https://www.licpathway.net/KnockTFv2/), ENCODE [32] (https://www.encodeproject.org/), hTFtarget [33] (http://bioinfo.life.hust.edu.cn/hTFtarget), GTRD [34] (https://gtrd.biouml.org/), and ChIP-Atlas [35] (https://chip-atlas.org/). Based on these results, the JASPAR [36] database (https://jaspar.elixir.no/) was further used to perform motif scanning of the ALOX5 promoter region and predict potential c-Myc binding sites.

Macrophage co-culture assay

THP-1 monocytes were differentiated into M0 macrophages by a 24-hour exposure to 100 nM phorbol 12-myristate 13-acetate (PMA) under standard culture conditions to ensure uniform morphology. Two Transwell co-culture systems were established using ccRCC cell lines (786-O or 769-P) expressing either sh-ALOX5 or a control. In the non-contact co-culture configuration, 0.4 μm pore inserts (Corning) were used, with tumor cells seeded in the upper chamber and macrophages in the lower chamber. For macrophage migration assays, 8 μm pore inserts (Corning) were employed, with macrophages seeded in the upper chamber and tumor cells in the lower chamber.

Both systems were cultured at 37°C, 5% CO_2 for 24 h. Following incubation, the macrophages were harvested for total RNA isolation. Following this, a quantitative real-time polymerase chain reaction (qRT-PCR) was employed to gauge the mRNA expression of pivotal indicators linked to M1 and M2 macrophage polarization, thereby enabling a thorough assessment of the polarization state.

Animal experiments

Stable 769-P cells expressing sh-ALOX5 or sh-Ctrl were harvested, counted, and resuspended in sterile PBS (5×10^6 cells/100 μL per mouse). The cell suspension was injected subcutaneously into the right axillary region of 6-week-old female BALB/c nude mice. Specific-pathogen-free mice, purchased from the Shanghai Model Organisms Center, were randomly assigned to two groups (n = 6 per group). One mouse in each group failed to develop a palpable tumor following subcutaneous injection and was excluded from subsequent analyses, resulting in a final sample size of n = 5 per group. Mice were maintained under controlled conditions (temperature: 22 ± 2°C, humidity: 50-60%, 12 h light/dark cycle) with free access to standard chow and water. Tumor growth was monitored every three days using caliper measurements of tumor length and width, and tumor volume was calculated as $V = (L \times W^2)/2$. Body weight was measured throughout the study. Mice were euthanized at week 4 or when humane endpoint criteria (tumor volume > 1500 mm^3, ulceration, or impaired mobility) were met, using CO_2 inhalation (20-30% chamber volume displacement per minute). Cessation of vital signs was confirmed before tumor excision. Tumors were weighed, photographed, and a portion was fixed in 4% paraformaldehyde for paraffin embedding and immunohistochemical analysis. All animal procedures and experiments were approved by the Institutional Animal Care and Use Committee (IACUC) of Shanghai Novopathway Biotechnology Co., Ltd. (Approval No. P0820251108A).

Statistical analysis

Statistical differences were assessed by two-tailed t-test for two groups, or one-way ANOVA with Tukey's post hoc test for multiple groups. For experiments involving repeated measurements of the same samples over time across multiple groups, including CCK-8 proliferation assays and in vivo tumor growth curves, two-way repeated-measures ANOVA was applied. Survival analyses were performed using Kaplan-Meier curves followed by log-rank test. Correlations were assessed using Pearson's or Spearman's correlation coefficient as appropriate, with the specific method indicated in each corresponding figure; $P < 0.05$ was considered statistically significant. All analyses were conducted using GraphPad Prism 9.0 or R 4.2.1. Data are presented as mean ± SD from at least three independent replicates.

Additional materials and methods can be found in the Supplementary Materials.

Results

High expression of ALOX5 in ccRCC predicts poor prognosis

To explore the potential importance of ALOX5 in renal cell carcinoma, we first performed bioinformatic analysis based on public databases. Increased ALOX5 expression in mRNA level was observed in tumor tissues compared with that of the normal kidney tissues according to the TCGA-KIRC dataset (**Figure 1A**). When comparing tumor tissues with adjacent non-tumor tissues, a similar trend was observed (**Figure 1B**). Meanwhile, ALOX5 expression was significantly upregulated across all tumor stages (T1-T4) compared to normal tissues (**Figure 1C**). This was further supported by four independent GEO datasets (GSE46699, GSE40435, GSE53757, and GSE15641), all showing substantial ALOX5 elevation in ccRCC specimens (**Figure 1D-G**). Protein-level analysis via the UALCAN database also confirmed markedly higher ALOX5 expression in ccRCC versus normal renal tissues (**Figure 1H**). Pan-cancer analysis of TCGA data revealed ALOX5 upregulation in various malignancies, including KIRC (Figure S1A).

Further validation in six paired clinical ccRCC and adjacent normal tissues showed significantly higher ALOX5 expression at both mRNA and protein levels, confirmed by qRT-PCR and Western blot (**Figure 1I**, **1J**). Among ccRCC cell lines (769-P, OS-RC-2, 786-O, and Caki-1), ALOX5 expression was notably higher than in normal HK-2 cells, with 769-P and 786-O showing the most pronounced upregulation, and thus selected for further *in vitro* studies (**Figure 1K**, **1L**).

Kaplan-Meier survival analysis revealed that high ALOX5 expression was significantly associated with poorer overall and disease-specific survival (**Figure 1M**, **1N**; log-rank test, $P < 0.05$). ROC analysis demonstrated ALOX5's strong diagnostic potential for ccRCC, with an AUC of 0.872 (95% CI: 0.827-0.918) (**Figure 1O**). Furthermore, TCGA-KIRC clinical data revealed that patients with high ALOX5 expression had significantly higher rates of lymph node metastasis (N1 stage: 5.0% vs. 1.2%, $P = 0.030$) and distant metastasis (M1 stage: 9.4% vs. 6.1%, $P = 0.041$) compared to low-expression patients (Table S4).

ALOX5 promotes proliferation, migration, and invasion of ccRCC cells

To examine ALOX5 function in ccRCC, we established stable ALOX5-deficient 786-O and 769-P cells using lentiviral transduction. qRT-PCR and Western blot methods both demonstrated a notable decrease in ALOX5 mRNA and protein abundance post-infection (**Figure 2A**, **2B**). CCK-8 evaluations showed significant reduction in 786-O and 769-P cell proliferation due to ALOX5 suppression (**Figure 2C**). As shown in (**Figure 2D**, **2E**), the migratory and invasive abilities of ALOX5-silenced cells were significantly impaired compared to the control group. Wound healing assays further revealed that ALOX5 depletion caused a marked delay in cell migration (**Figure 2F**). Understanding that the epithelial-to-mesenchymal transition (EMT) is pivotal in the process of cancer cells spreading and taking root elsewhere, we evaluated the EMT-associated markers at both the RNA and protein stages. Our findings revealed that decreasing ALOX5 expression led to a boost in the expression of the epithelial protein E-cadherin, while the levels of the mesenchymal proteins N-cadherin and Vimentin were notably diminished (**Figure 2G**, **2H**). Collectively, these results indicate that ALOX5 stimulates ccRCC cell growth, movement, infiltration, and epithelial-mesenchymal transition, demonstrating oncogene-like properties.

ALOX5 knockdown suppresses tumorigenicity of ccRCC in vivo

To substantiate ALOX5's oncogenic potential *in vivo*, subcutaneous xenografts employing 769-P cells with stable sh-ALOX5 or control vector transduction were investigated. ALOX5 knockdown markedly suppressed tumor proliferation, significantly decreasing both volume and mass relative to controls (**Figure 3A-C**). Immunohistochemical analysis indicated reduced levels of ALOX5, the proliferative marker Ki-67, and the protein associated with metastasis, Vimentin, in tumors from the sh-ALOX5 cohort (**Figure 3D**).

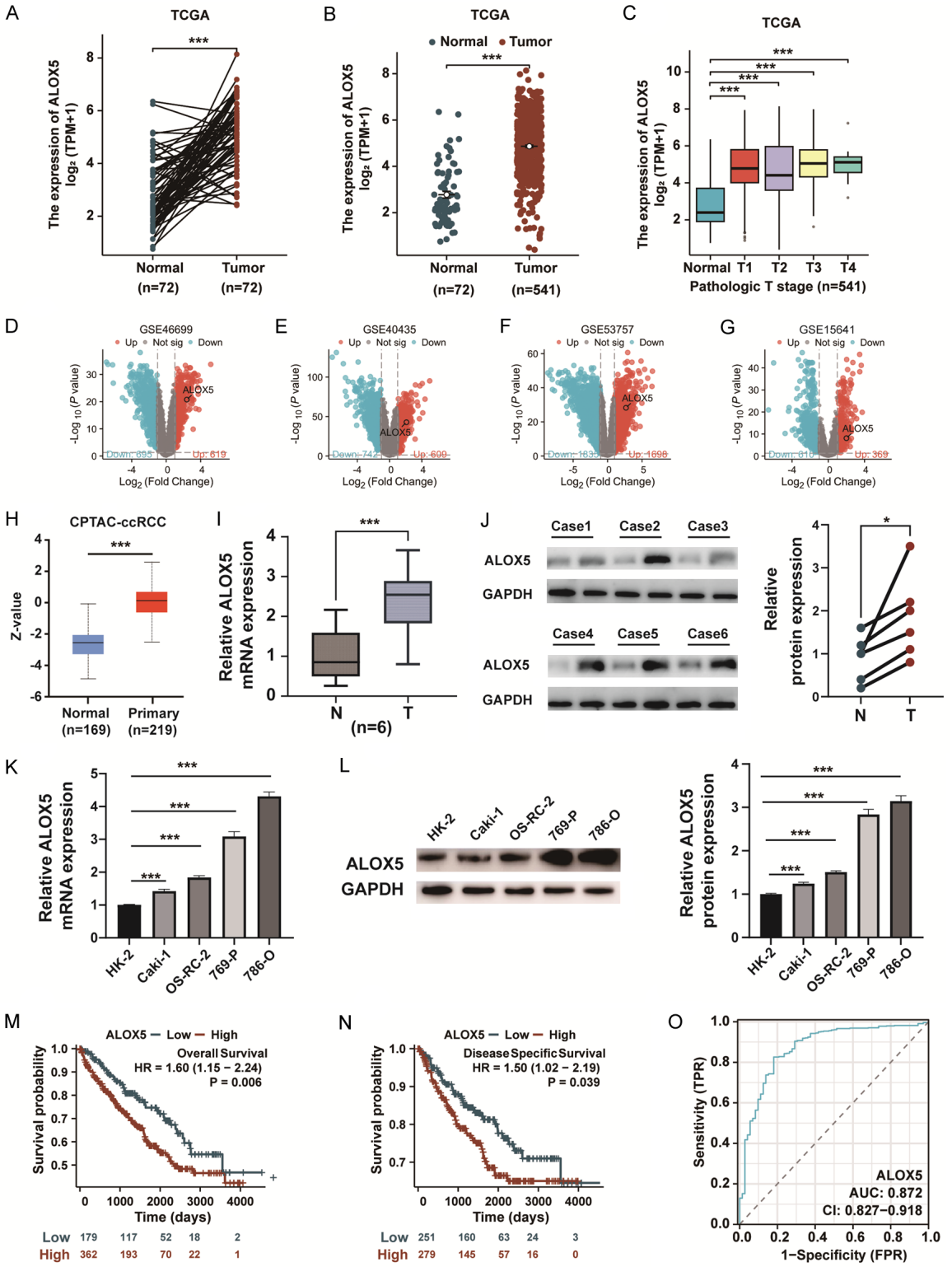

Figure 1. ALOX5 is highly expressed in ccRCC and associated with poor prognosis. A. Expression of ALOX5 in paired tumor and adjacent normal tissues from the TCGA-KIRC cohort. B. Differential ALOX5 expression between tumor and normal tissues in the TCGA-KIRC dataset. C. ALOX5 expression stratified by pathological T stage (T1-T4). D-G. Comparison of ALOX5 expression between tumor and normal tissues across four independent GEO datasets (GSE46699, GSE40435, GSE53757, and GSE15641). H. Protein expression of ALOX5 in ccRCC samples based on the UALCAN (CPTAC) database. I. Relative ALOX5 mRNA expression in six pairs of ccRCC and adjacent normal tis-

sues detected by qRT-PCR. J. Representative Western blot (WB) images showing ALOX5 protein levels in six paired clinical samples. K, L. qRT-PCR and WB analyses showing increased ALOX5 mRNA and protein levels in renal cancer cell lines (Caki-1, OS-RC-2, 769-P, and 786-O) compared with the normal renal epithelial cell line HK-2. M, N. Kaplan-Meier survival curves for overall survival (OS) and disease-specific survival (DSS) in the TCGA-KIRC cohort grouped by high and low ALOX5 expression. O. Receiver operating characteristic (ROC) curve analysis evaluating the diagnostic performance of ALOX5 expression in distinguishing tumor tissues from adjacent normal tissues. *P < 0.05, **P < 0.01, ***P < 0.001.

ALOX5 inhibition impairs macrophage chemotaxis and M2 polarization

Earlier research has pointed to ALOX5's involvement in modulating tumor-associated macrophages (TAMs) across different cancer types. When examining the TCGA-KIRC dataset, it became evident that ALOX5 expression levels and macrophage presence in ccRCC tissues go hand in hand, showing a strong positive link (R = 0.465, P < 0.001; **Figure 4A**). Furthermore, ALOX5 levels were associated with the presence of M2 macrophage indicators CD163 and CD206 (**Figure 4B**, **4C**). To experimentally confirm whether ALOX5 mediates the interaction between ccRCC cells and macrophages, we co-cultured THP-1-derived macrophages with ALOX5-knockdown (or control) 786-O and 769-P cells (**Figure 4D**). Co-culture with ccRCC cells enhanced the migration of THP-1 macrophages toward the lower chamber, while ALOX5 knockdown significantly attenuated this chemotactic response (**Figure 4E**). PCR analysis demonstrated an upregulated expression of M2 markers (CD163 and CD206) in macrophages co-cultured with 786-O and 769-P, indicating tumor-driven macrophage polarization (**Figure 4F**). Meanwhile, ALOX5 knockdown in 786-O cells significantly reduced the expression of M2-associated genes (CD163, CD206, Arg-1, and IL-10) in co-cultured macrophages (**Figure 4G**). WB analysis further confirmed the above phenotype, showing that ALOX5 depletion markedly decreased the protein levels of CD206 and Arg-1, which are also typical M2 macrophage markers (**Figure 4H**). Together, the above results suggest that ALOX5 facilitates macrophage infiltration and promotes ccRCC cells' ability in inducing macrophage M2 polarization into TAMs within the ccRCC tumor microenvironment.

c-Myc directly promotes transcriptional activation of ALOX5

Given that transcriptional regulation is a fundamental driver of oncogenic initiation and progression, we sought to elucidate the molecular mechanism underlying ALOX5 upregulation. To this end, we integrated data from five authoritative transcription factor (TF) databases including KnockTF, ENCODE, GTRD, hTFtarget, and ChIP-Atlas. The intersection identified four candidate TFs after performing Venn analysis: CTCF, GATA1, c-Myc, and RNF2 (**Figure 5A**). Among them, c-Myc is a well-characterized transcription factor known to recognize E-box motifs and transcriptionally activate a broad range of genes associated with proliferation and metabolism. Analysis of the TCGA-KIRC cohort showed that c-Myc exhibited the most pronounced upregulation among these candidates and displayed the strongest positive correlation with ALOX5 expression (R = 0.306; **Figure 5B-D**; Figure S1B, S1C). To validate this regulatory relationship, we silenced c-Myc in 786-O and 769-P cells, and both ALOX5 mRNA and protein levels were significantly reduced following c-Myc knockdown (**Figure 5E**, **5F**). Motif prediction using the JASPAR database identified three potential c-Myc-binding sites within the ALOX5 promoter region (**Figure 5G**, **5H**). ChIP-qPCR assays demonstrated that binding site 1 showed the highest enrichment of c-Myc, suggesting it as the major occupancy locus (**Figure 5I**). Moreover, the dual-luciferase reporter tests indicated a substantial boost in the transcriptional efficacy of the ALOX5 promoter due to c-Myc, yet mutating the crucial binding site significantly attenuated this activation (**Figure 5J**). Taken together, these findings demonstrate that c-Myc directly binds to and transcriptionally activates the ALOX5 promoter, leading to its upregulation. The combined evidence from bioinformatic screening, ChIP and luciferase assays consistently provided sound evidence to this direct regulatory relationship.

The c-Myc-ALOX5 axis promotes malignant phenotypes of ccRCC cells and TAM polarization

According to the above observation and analysis where c-Myc transcriptionally upregulates ALOX5, we hypothesized that c-Myc may drive

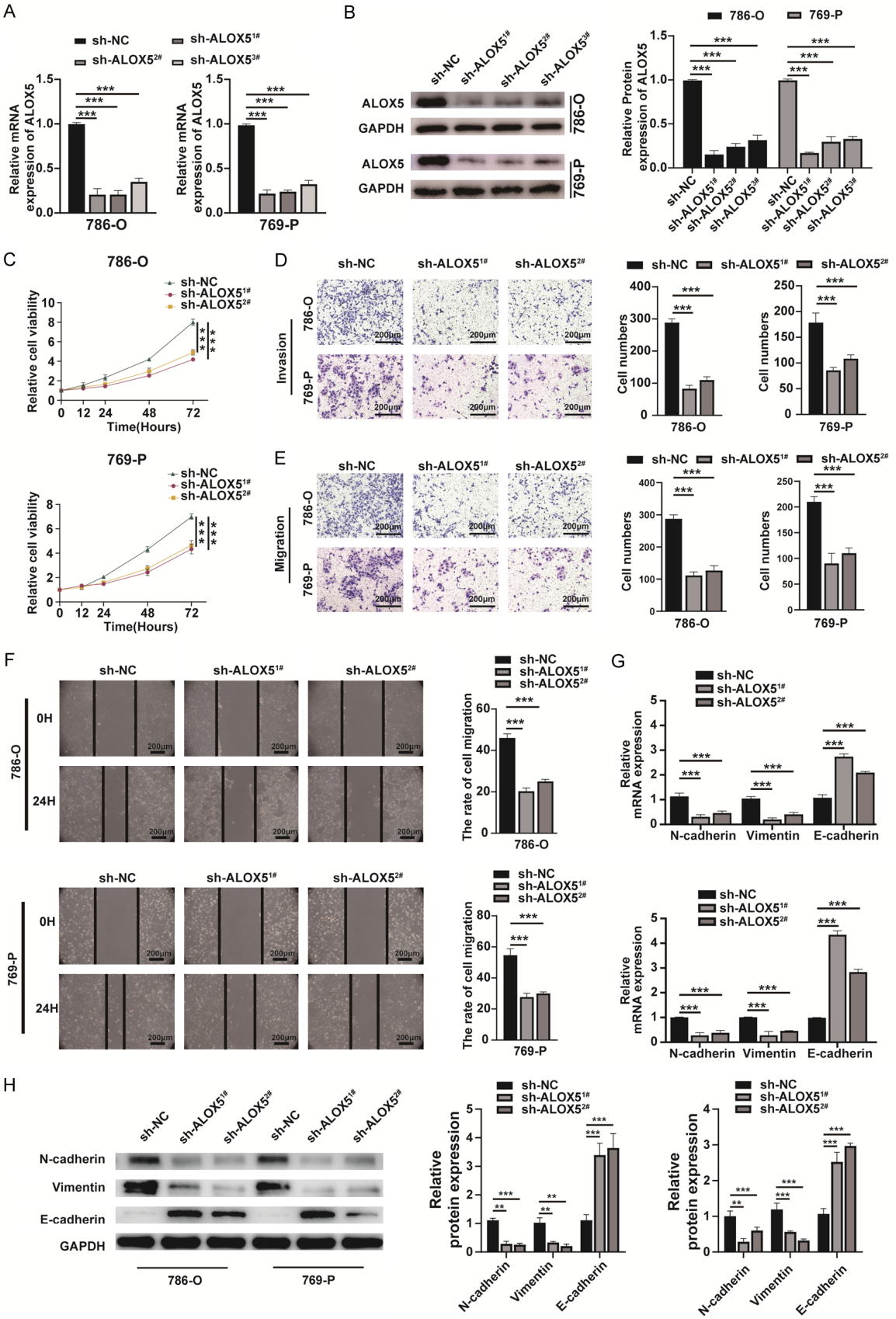
A
sh-NC
sh-ALOX5$^{1\#}$
sh-ALOX5$^{2\#}$
sh-ALOX5$^{3\#}$
Relative mRNA expression of ALOX5
786-O
769-P
B
ALOX5
GAPDH
786-O
769-P
Relative Protein expression of ALOX5
C
786-O
769-P
Relative cell viability
Time(Hours)
D
Invasion
Cell numbers
E
Migration
F
0H
24H
The rate of cell migration
G
Relative mRNA expression
N-cadherin
Vimentin
E-cadherin
H
Relative protein expression

Figure 2. ALOX5 promotes the proliferation, migration, and invasion of ccRCC cells. (A, B) Validation of ALOX5 knockdown efficiency by qRT-PCR and Western blot (WB) analysis. (C) CCK-8 assay results showing that ALOX5 knockdown suppressed cell proliferation in 769-P and 786-0 cells. (D, E) Transwell invasion and migration assays demonstrating that ALOX5 knockdown significantly reduced the migratory and invasive capacities of ccRCC cells (magnification, ×100). (F) Wound-healing assays evaluating the migratory ability of ALOX5-knockdown cells, with quantitative analysis of wound closure (magnification, ×200). (G) qRT-PCR analysis of EMT-related markers, including E-cadherin, N-cadherin, and Vimentin, in ALOX5-knockdown ccRCC cells. (H) Western blot analysis of E-cadherin, N-cadherin, and Vimentin protein levels in ALOX5-knockdown ccRCC cells, with densitometric quantification. *P < 0.05, **P < 0.01, ***P < 0.001. Cell proliferation in (C) was analyzed using two-way repeated-measures ANOVA.

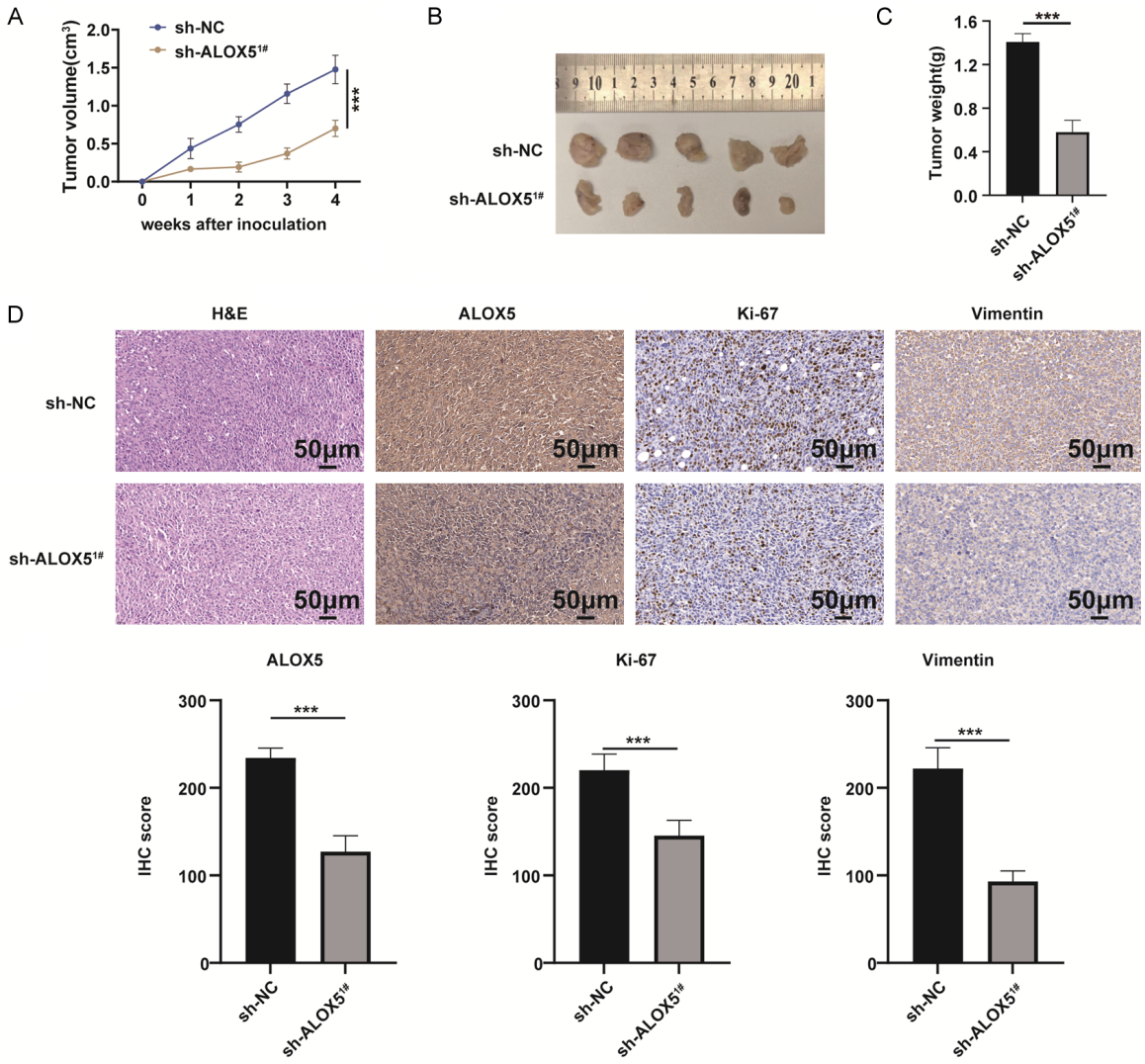

Figure 3. Knockdown of ALOX5 suppresses the tumorigenicity of ccRCC *in vivo*. (A) Tumor growth curves of subcutaneous xenografts derived from 769-P cells (5 × 10^6) transduced with sh-Ctrl or sh-ALOX5 lentivirus (n = 6 mice injected per group; n = 5 per group included in analysis after exclusion of one non-tumor-forming mouse per group). (B) Representative images of excised tumors at day 28 post-implantation. (C) Comparison of tumor weights at the experimental endpoint (day 28). (D) Representative hematoxylin and eosin (H&E) and immunohistochemical (IHC) staining of xenograft tissues showing ALOX5, Ki-67, and Vimentin expression, along with corresponding IHC scores (magnification, ×400). *P < 0.05, **P < 0.01, ***P < 0.001. Tumor volume in (A) was analyzed using two-way repeated-measures ANOVA.

the progression of ccRCC via the ALOX5 pathway. To test this hypothesis, ALOX5 overexpression plasmids were constructed and transfected into 786-0 and 769-P cells, with successful

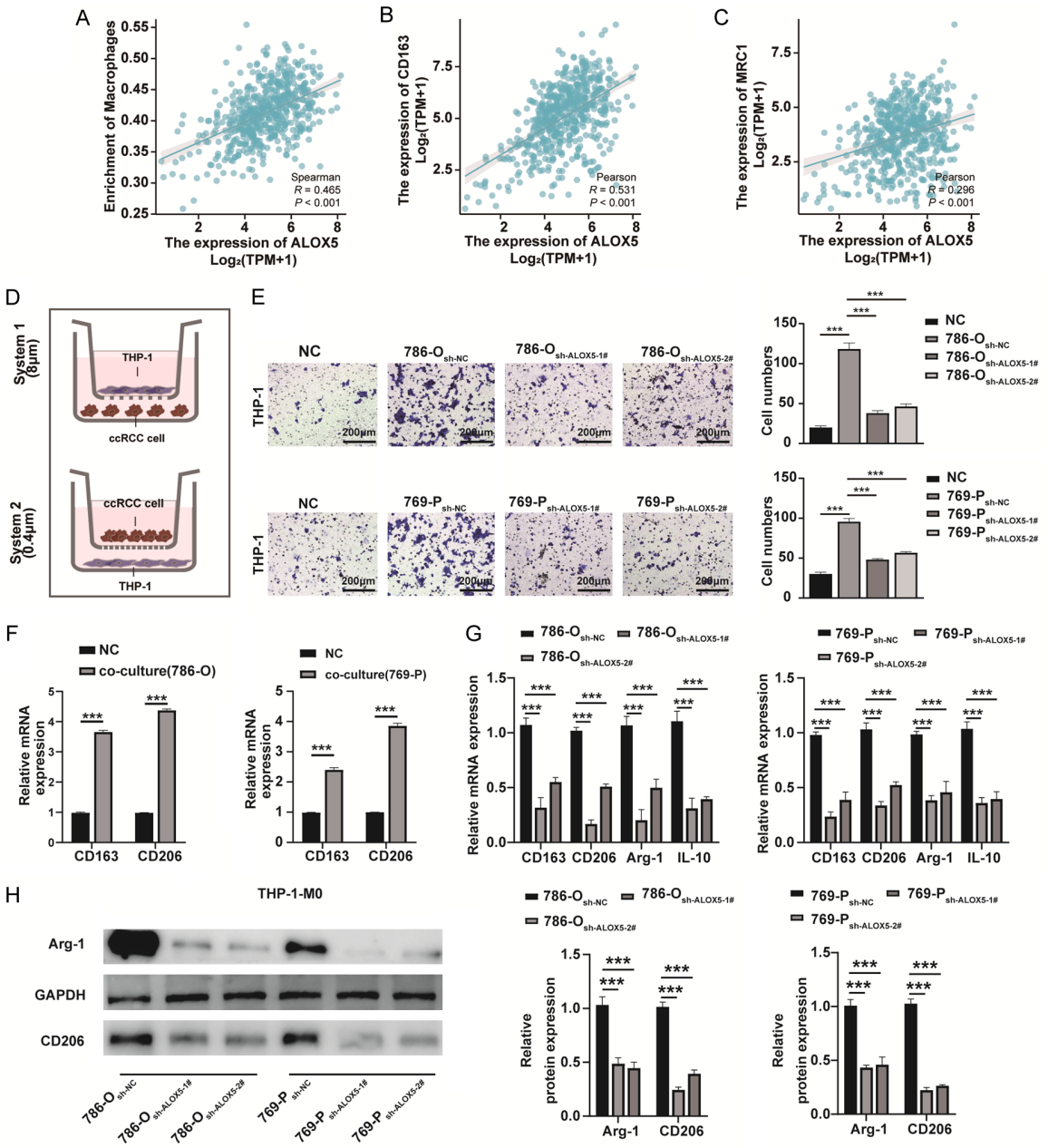

Figure 4. Inhibition of ALOX5 affects the chemotaxis and M2 polarization of THP-1-derived macrophages. A. Correlation analysis between ALOX5 expression and macrophage infiltration levels based on the TCGA-KIRC dataset. B, C. Correlation of ALOX5 expression with CD163 and MRC1 (CD206) in the TCGA database. D. Schematic illustration of the Transwell co-culture system: system 1 (tumor cells seeded in the lower chamber for macrophage recruitment) and system 2 (tumor cells in the upper chamber for macrophage polarization). E. Transwell migration assay evaluating the effect of ALOX5 on the chemotactic recruitment of THP-1-derived M0 macrophages (magnification, ×100). F. qRT-PCR analysis of M2 markers (CD206 and CD163) in THP-1-M0 macrophages co-cultured with 769-P or 786-O cells. G. qRT-PCR analysis of M2-associated genes (CD163, CD206, Arg-1, and IL-10) in THP-1-derived macrophages after co-culture with NC, 786-O, or ALOX5-knockdown 786-O cells. H. Western blot analysis and quantification of M2-associated proteins, including CD206 and Arg-1. *$P < 0.05$, **$P < 0.01$, ***$P < 0.001$.

overexpression confirmed by qRT-PCR and WB analyses (Figure S1D, S1E). Cells were then transfected with sh-c-Myc alone or co-transfected with oe-ALOX5 to evaluate their combined effects. As shown in (**Figure 6A**, **6B**), suppressing c-Myc markedly reduced cell growth, movement, and infiltration, whereas ALOX5 upregulation partly counteracted these out-

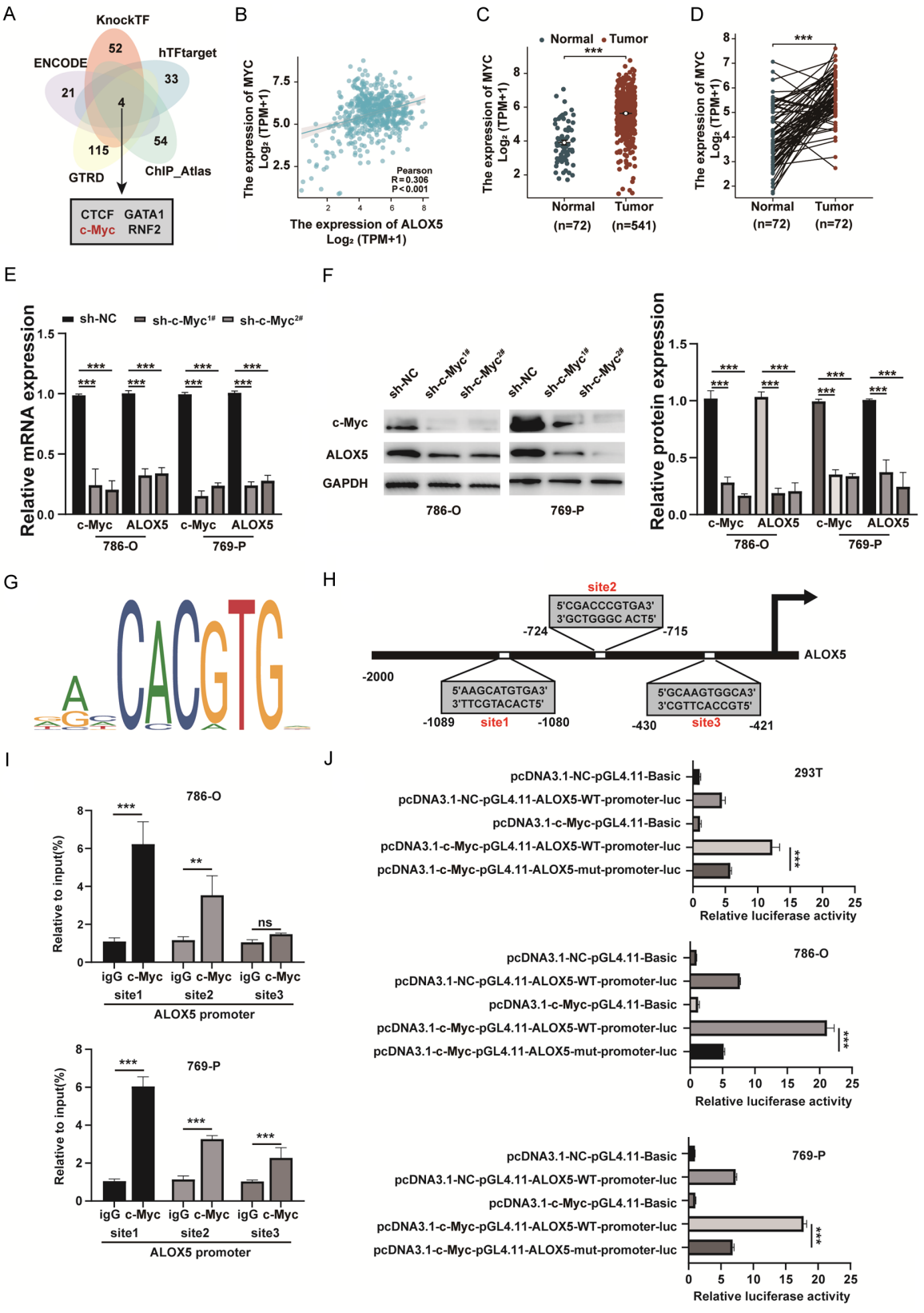

Figure 5. c-Myc directly promotes the transcriptional activation of ALOX5. A. Venn diagram showing the predicted transcription factors (TFs) of ALOX5 based on five databases: KnockTF, ENCODE, hTFtarget, GTRD, and ChIP-Atlas. B. Scatter plot showing the correlation between c-Myc and ALOX5 expression in the TCGA-KIRC cohort. C, D. TCGA-

KIRC data indicating upregulated c-Myc transcripts in both paired and unpaired ccRCC samples. E, F. qRT-PCR and Western blot (WB) analyses showing the effects of c-Myc silencing on ALOX5 mRNA and protein expression in ccRCC cells. G. Predicted c-Myc-binding sites within the ALOX5 promoter region based on the JASPAR database. H. Schematic diagram of three potential c-Myc-binding motifs on the ALOX5 promoter. I. ChIP-qPCR analysis confirming c-Myc enrichment at the predicted binding sites within the ALOX5 promoter in 786-O and 769-P cells. J. Dual-luciferase reporter assays showing that mutation of the first c-Myc-binding site significantly decreased ALOX5 promoter-driven luciferase activity in 786-O, 769-P, and 293T cells compared with the wild-type promoter. *$P < 0.05$, **$P < 0.01$, ***$P < 0.001$.

comes. Accordingly, c-Myc depletion decreased EMT gene expression at both mRNA and protein levels, which was partially recovered after ALOX5 overexpression (**Figure 6C**, **6D**). Moreover, the analysis on TCGA-KIRC dataset also demonstrated a direct link between c-Myc levels and the presence of macrophages, and also to the M2 macrophage biomarkers, specifically CD163 and CD206 (Figure S1F-H).

In co-culture experiments, c-Myc knockdown in ccRCC cells significantly reduced macrophage recruitment, while ALOX5 overexpression restored the migration of THP-1-derived macrophages in the co-culture systems (**Figure 6E**). c-Myc suppression led to the downregulation of M2 polarization markers - such as CD163, CD206, Arg-1, and IL-10 - and a significant reduction in CD206 fluorescence in tumor-associated macrophages (TAMs). Notably, these effects were partially reversed by ALOX5 overexpression (**Figure 6F**, **6G**).

In conclusion, the data suggest that the c-Myc-ALOX5 signaling pathway promotes the aggressive progression of ccRCC through multiple mechanisms, including enhancing tumor cell proliferation, migration, and invasion, as well as facilitating macrophage recruitment and M2 polarization in the tumor immune microenvironment.

Discussion

Clear cell renal cell carcinoma (ccRCC) is the most common pathological subtype of renal cancer. While the five-year survival rate for early-stage renal cancer remains relatively favorable, the prognosis for renal cancer patients overall remains poor, particularly for those with advanced and metastatic disease [37]. Targeted therapies and immunotherapy have provided new hope for patients with advanced ccRCC, but the challenge of resistance continues to hinder patient outcomes. The precise molecular mechanisms underlying the development and progression of renal cancer, particularly the functions of key oncogenes associated with metabolic regulation, remain incompletely understood. This study is the first to identify ALOX5, a lipid-metabolizing enzyme, as a critical oncogene in ccRCC progression. ALOX5 not only promotes the malignant features of tumor cells but also contributes to immune evasion by modulating the tumor immune microenvironment (TIME). We found that elevated ALOX5 levels in ccRCC tissues and cell lines were strongly correlated with adverse clinical outcomes. We experimentally demonstrated that ALOX5 inhibition significantly suppressed ccRCC malignant phenotype including tumor cell growth, migration, invasion, and the EMT, indicating ALOX5's direct role in ccRCC both *in vitro* and *in vivo*. Furthermore, increased ALOX5 expression was proved to contribute to enhanced tumor-infiltrating macrophage abundance and M2 polarization, suggesting that ALOX5 not only directly fuels ccRCC growth but also enhances tumor-immune cell interactions by remodeling the TIME, thereby facilitating immune escape.

Multiple studies have demonstrated the involvement of ALOX5 in the progression of various malignancies. For instance, ALOX5 activates the JAK/STAT signaling pathway to promote the M2 polarization of tumor-associated macrophages (TAMs), thereby enhancing tumor invasiveness and metastatic transfer in pancreatic cancer [13]. In glioma, ALOX5 promotes 5-HETE-mediated M2 polarization and PD-L1 expression in glioma-associated microglia/macrophages [12]. Additionally, ALOX5 plays a protumorigenic role in colorectal cancer and leukemia, with inhibitors showing promising therapeutic potential in preclinical studies [38, 39]. However, the specific function and regulatory mechanisms of ALOX5 in renal cancer remain unclear. This study is the first to reveal ALOX5's role in ccRCC progression and to confirm that it facilitates malignant transformation through coordinating the regulation of both tumor cell phenotype and the immune microenvironment.

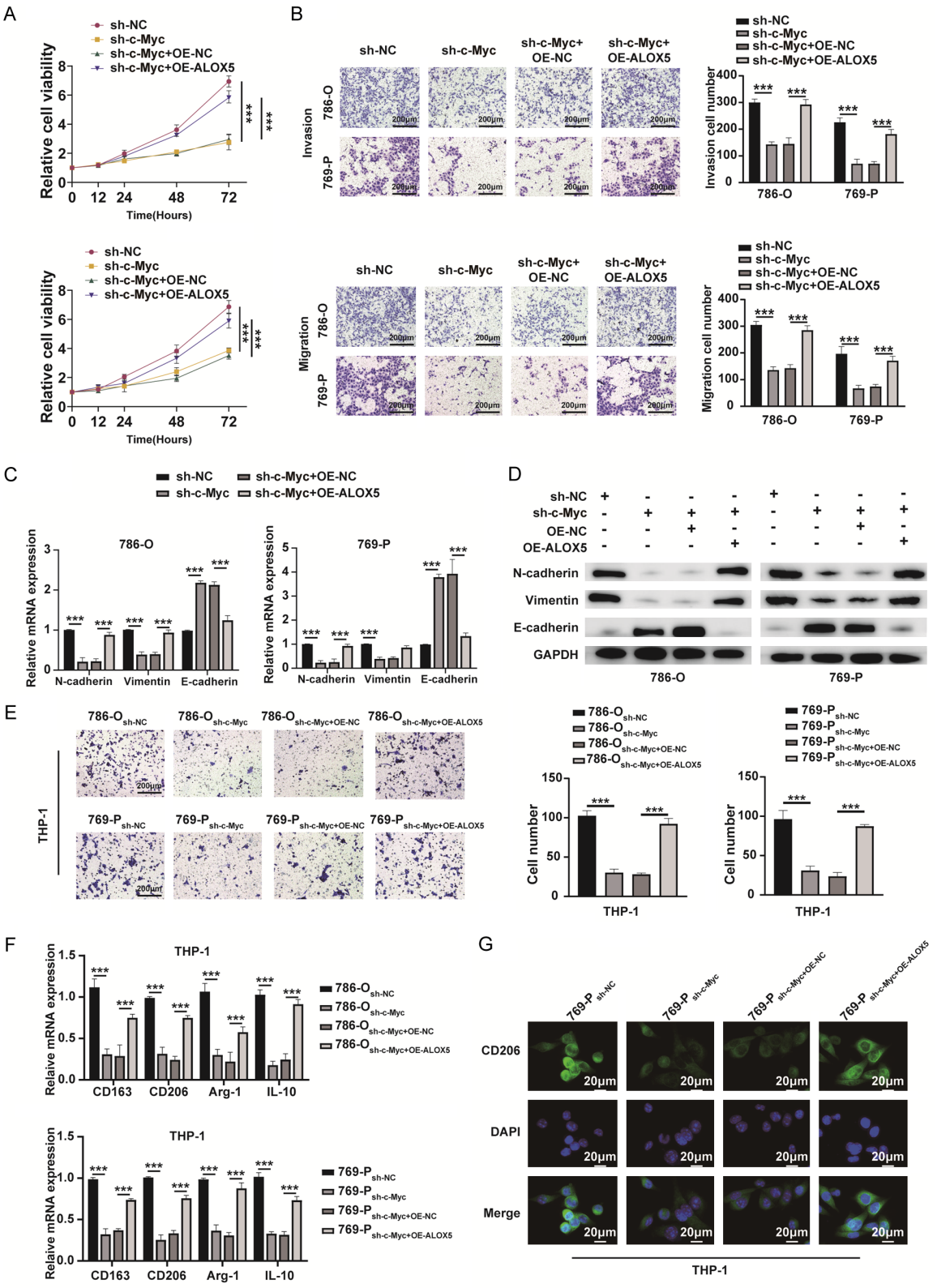

Figure 6. The c-Myc-ALOX5 axis promotes malignant phenotypes of ccRCC and drives TAMs toward M2 polarization. (A) CCK-8 assays quantifying the proliferation of 786-O and 769-P cells under c-Myc knockdown or control conditions, and the rescue effect of ALOX5 re-expression in the c-Myc-deficient background. (B) Transwell invasion and migration assays comparing the migratory and invasive capacities of c-Myc-knockdown and ALOX5-rescued cells (magnification, ×100). (C, D) qRT-PCR and Western blot (WB) analyses showing the expression changes of

epithelial-mesenchymal transition (EMT) markers (N-cadherin, Vimentin, and E-cadherin) under c-Myc knockdown and ALOX5 re-expression conditions. (E) Transwell co-culture assays assessing the effects of these conditions on the chemotactic recruitment of THP-1-derived M0 macrophages (magnification, ×100). (F) qRT-PCR analysis of M2 macrophage markers (CD163, CD206, Arg-1, and IL-10) in co-cultured THP-1 macrophages. (G) Immunofluorescence staining of CD206 (green) in co-cultured THP-1 macrophages, with DAPI nuclear counterstaining (blue) (magnification, ×1000). *$P < 0.05$, **$P < 0.01$, ***$P < 0.001$. Cell proliferation in (A) was analyzed using two-way repeated-measures ANOVA.

The tumor immune microenvironment plays a critical role in ccRCC progression, particularly through the influence of TAMs [40, 41]. TAMs can be broadly categorized into M1 (anti-tumor) and M2 (pro-tumor) macrophages. M2 macrophages promote tumor progression, angiogenesis, and immune evasion by secreting immunosuppressive cytokines such as IL-10 and Arg-1 [42, 43]. Our study found a strong correlation between ALOX5 expression and TAM infiltration as well as M2 macrophage differentiation. Knockdown of ALOX5 significantly impaired the chemotaxis and polarization of THP-1-derived macrophages. Consistent with its immunomodulatory role in other types of cancer, our findings suggest that ALOX5 not only directly participates in the malignant behavior of ccRCC cells, but also enhances immune evasion by remodulating the immune cell composition.

Mechanistically, our study demonstrates that the classical oncogene transcription factor c-Myc directly binds to and activates the transcription of the ALOX5 promoter, thereby driving its upregulation. As a well-known oncogene, c-Myc regulates cellular metabolism, proliferation, and immune modulation in various cancers [44, 45]. Our ChIP-qPCR and dual-luciferase reporter assays, together with downstream functional rescue experiments confirmed the direct transcriptional regulation of ALOX5 by c-Myc and revealed the cooperative oncogenic effect of the c-Myc-ALOX5 axis in ccRCC. Moreover, considering the established role of c-Myc in immune evasion in renal cancer, our study provides novel mechanistic insights by showing that c-Myc promotes M2 polarization of TAMs via ALOX5, thereby contributing to the establishment of the immunosuppressive tumor microenvironment in ccRCC. Our findings not only deepen the understanding of the biological mechanisms underlying ccRCC development but also highlight the therapeutic potential of targeting the c-Myc-ALOX5 axis.

However, acknowledgement of several limitations in this work is inevitable. First, while we validated the oncogenic function of ALOX5 both *in vitro* and *in vivo*, the specific contributions of its downstream lipid metabolites, such as 5-HETE and LTB4, to tumor progression have not been thoroughly investigated. Second, this study primarily used THP-1-derived macrophages as an *in vitro* model. While this model has been widely used in tumor microenvironment-related studies, the PMA-induced differentiation of monocytes into M0 macrophages is not the most direct source of macrophages, and the model's effectiveness may be somewhat limited. Future studies should validate these findings using primary immune cells and clinical samples. Finally, while we investigated the correlation between ALOX5 and ccRCC prognosis using publicly available databases, clinical samples from real-world settings are needed to further support these findings.

In conclusion, our study establishes the c-Myc-ALOX5 axis as a key driver of ccRCC progression, identifying ALOX5 as a crucial downstream effector of c-Myc that promotes M2 macrophage polarization and immune evasion. Targeting this signaling pathway may offer a breakthrough strategy for the treatment of ccRCC.

Acknowledgements

The authors would like to thank the Shanghai Health Commission Key Laboratory of Artificial Intelligence (AI)-Based Management of Inflammation and Chronic Diseases, as well as the Sino-French Cooperative Central Laboratory at Shanghai Pudong Gongli Hospital, for their technical and infrastructural support. We also thank the Department of Urology, Tongji Hospital, School of Medicine, Tongji University, for facilitating sample collection and clinical data acquisition. We are grateful to all patients who provided tissue samples for this study, and to all colleagues who contributed to data processing and manuscript preparation. This study was supported by the Research Grant for Health Science and Technology from the Pudong Health Bureau of Shanghai (Grant No. PW2023A-19) and the Shanghai Pudong New

District Science and Technology Innovation Project (PKJ2025-Y17).

The written informed consent was obtained from all participants.

Disclosure of conflict of interest

None.

Abbreviations

ccRCC, Clear Cell Renal Cell Carcinoma; ALOX5, Arachidonate 5-Lipoxygenase; TAMs, Tumor-Associated Macrophages; TIME, tumor immune microenvironment; c-Myc, c-Myc Proto-Oncogene BHLH Transcription Factor; EMT, Epithelial-Mesenchymal Transition; TCGA, The Cancer Genome Atlas; qRT-PCR, Quantitative Real-Time Polymerase Chain Reaction; GEO, Gene Expression Omnibus; ChIP, Chromatin Immunoprecipitation; IHC, Immunohistochemistry; STR, Short Tandem Repeat; BCA, Bicinchoninic Acid; ECL, Enhanced Chemiluminescence; HRP, Horseradish Peroxidase; OS, Overall Survival; DSS, Disease-Specific Survival; AUC, Area Under the Curve; ROC, Receiver Operating Characteristic.

Address correspondence to: Xue Zhang, Shanghai Health Commission Key Lab of Artificial Intelligence (AI)-Based Management of Inflammation and Chronic Diseases, Sino-French Cooperative Central Lab, Shanghai Pudong Gongli Hospital, No. 219 Miaopu Road, Pudong New Area, Shanghai 200135, China. E-mail: xue0221@139.com; Weidong Zhou and Denglong Wu, Department of Urology, Tongji Hospital, School of Medicine, Tongji University, No. 389 Xincun Road, Putuo District, Shanghai 200065, China. E-mail: 1811219@tongji.edu.cn (WDZ); wudenglong2009@tongji.edu.cn (DLW)

References

[1] Gulati S and Vaishampayan U. Current state of systemic therapies for advanced renal cell carcinoma. Curr Oncol Rep 2020; 22: 26.

[2] Hsieh JJ, Purdue MP, Signoretti S, Swanton C, Albiges L, Schmidinger M, Heng DY, Larkin J and Ficarra V. Renal cell carcinoma. Nat Rev Dis Primers 2017; 3: 17009.

[3] Rosellini M, Marchetti A, Mollica V, Rizzo A, Santoni M and Massari F. Prognostic and predictive biomarkers for immunotherapy in advanced renal cell carcinoma. Nat Rev Urol 2023; 20: 133-157.

[4] Choueiri TK and Motzer RJ. Systemic therapy for metastatic renal-cell carcinoma. N Engl J Med 2017; 376: 354-366.

[5] Xu J, Ding L, Mei J, Hu Y, Kong X, Dai S, Bu T, Xiao Q and Ding K. Dual roles and therapeutic targeting of tumor-associated macrophages in tumor microenvironments. Signal Transduct Target Ther 2025; 10: 268.

[6] Jiang W, Liu L, Xu Z, Qiu Y, Zhang B, Cheng J, Luo J, Qu Y, Guo J and Xu J. SPP1+ tumor-associated macrophages drive immunotherapy resistance via CD8+ T-cell dysfunction in clear-cell renal cell carcinoma. Cancer Immunol Res 2025; 13: 1533-1546.

[7] Pan XW, Zheng HF, Li MC, Dong KQ, Tang YF, Chen JX, Yang TY, Liu JG, Liu ZC, Liu Y, Li WY, Gong ZX, Zhang S, Zhou W, Gu J and Cui XG. Unveiling the mechanisms of CEBPD-orchestrated TAM polarization through RGS2/PAR2 pathway and its impact on ICB efficacy in clear cell renal cell carcinoma. J Immunother Cancer 2025; 13: e010898.

[8] Liu H, Lv Z, Zhang G, Yan Z, Bai S, Dong D and Wang K. Molecular understanding and clinical aspects of tumor-associated macrophages in the immunotherapy of renal cell carcinoma. J Exp Clin Cancer Res 2024; 43: 242.

[9] Zhuravlev A, Gavrilyuk V, Chen X, Aksenov V, Kuhn H and Ivanov I. Structural and functional biology of mammalian ALOX isoforms with particular emphasis on enzyme dimerization and their allosteric properties. Int J Mol Sci 2024; 25: 12058.

[10] Wenzel SE, Tyurina YY, Zhao J, St Croix CM, Dar HH, Mao G, Tyurin VA, Anthonymuthu TS, Kapralov AA, Amoscato AA, Mikulska-Ruminska K, Shrivastava IH, Kenny EM, Yang Q, Rosenbaum JC, Sparvero LJ, Emlet DR, Wen X, Minami Y, Qu F, Watkins SC, Holman TR, VanDemark AP, Kellum JA, Bahar I, Bayır H and Kagan VE. PEBP1 wardens ferroptosis by enabling lipoxygenase generation of lipid death signals. Cell 2017; 171: 628-641, e626.

[11] Yang WS, Kim KJ, Gaschler MM, Patel M, Shchepinov MS and Stockwell BR. Peroxidation of polyunsaturated fatty acids by lipoxygenases drives ferroptosis. Proc Natl Acad Sci U S A 2016; 113: E4966-E4975.

[12] Chen T, Liu J, Wang C, Wang Z, Zhou J, Lin J, Mao J, Pan T, Wang J, Xu H, He X, Wu D and Liu Z. ALOX5 contributes to glioma progression by promoting 5-HETE-mediated immunosuppressive M2 polarization and PD-L1 expression of glioma-associated microglia/macrophages. J Immunother Cancer 2024; 12: e009492.

[13] Hu WM, Liu SQ, Zhu KF, Li W, Yang ZJ, Yang Q, Zhu ZC and Chang J. The ALOX5 inhibitor Zileuton regulates tumor-associated macrophage M2 polarization by JAK/STAT and inhibits pan-

creatic cancer invasion and metastasis. Int Immunopharmacol 2023; 121: 110505.
[14] Ji Z, Li X, Gao W, Xia Q and Li J. ALOX5 induces EMT and promotes cell metastasis via the LTB4/BLT2/PI3K/AKT pathway in ovarian cancer. Cell Signal 2024; 124: 111404.
[15] Zhou X, Jiang Y, Li Q, Huang Z, Yang H and Wei C. Aberrant ALOX5 activation correlates with HER2 status and mediates breast cancer biological activities through multiple mechanisms. Biomed Res Int 2020; 2020: 1703531.
[16] Liu T, Xu X, Li J, Bai M, Zhu W, Liu Y, Liu S, Zhao Z, Li T, Jiang N, Bai Y, Jin Q, Zhang Y, Zheng Y, Zhou S, Zhan S, Sun Y, Liang G, Luo Y, Chen X, Guo H and Yang R. ALOX5 deficiency contributes to bladder cancer progression by mediating ferroptosis escape. Cell Death Dis 2023; 14: 800.
[17] Chen J, Tang Y, Qin D, Yu X, Tong H, Tang C and Tang Z. ALOX5 acts as a key role in regulating the immune microenvironment in intrahepatic cholangiocarcinoma, recruiting tumor-associated macrophages through PI3K pathway. J Transl Med 2023; 21: 923.
[18] Dhanasekaran R, Deutzmann A, Mahauad-Fernandez WD, Hansen AS, Gouw AM and Felsher DW. The MYC oncogene - the grand orchestrator of cancer growth and immune evasion. Nat Rev Clin Oncol 2022; 19: 23-36.
[19] Duffy MJ, O'Grady S, Tang M and Crown J. MYC as a target for cancer treatment. Cancer Treat Rev 2021; 94: 102154.
[20] Sun L, He M, Li F, Wu D, Zheng P, Zhang C, Liu Y, Liu D, Shan M, Yang M, Ma Y, Lian J and Xiong H. Oxyberberine sensitizes liver cancer cells to sorafenib via inhibiting NOTCH1-USP7-c-Myc pathway. Hepatol Commun 2024; 8: e0405.
[21] Lourenco C, Resetca D, Redel C, Lin P, MacDonald AS, Ciaccio R, Kenney TMG, Wei Y, Andrews DW, Sunnerhagen M, Arrowsmith CH, Raught B and Penn LZ. MYC protein interactors in gene transcription and cancer. Nat Rev Cancer 2021; 21: 579-591.
[22] Jing Z, Liu Q, He X, Jia Z, Xu Z, Yang B and Liu P. NCAPD3 enhances Warburg effect through c-myc and E2F1 and promotes the occurrence and progression of colorectal cancer. J Exp Clin Cancer Res 2022; 41: 198.
[23] Whitfield JR and Soucek L. MYC in cancer: from undruggable target to clinical trials. Nat Rev Drug Discov 2025; 24: 445-457.
[24] Zhang X, Chen Z, He X, Wang J, Zhong J, Zou Y, Zheng X, Lin Y, Zhang R, Kang T, Zhou L and Wu Y. SUMOylation of SETD8 promotes tumor growth by methylating and stabilizing myc in bladder cancer. Adv Sci (Weinh) 2025; 12: e2501734.
[25] Eckel-Passow JE, Serie DJ, Bot BM, Joseph RW, Cheville JC and Parker AS. ANKS1B is a smoking-related molecular alteration in clear cell renal cell carcinoma. BMC Urol 2014; 14: 14.
[26] Wozniak MB, Le Calvez-Kelm F, Abedi-Ardekani B, Byrnes G, Durand G, Carreira C, Michelon J, Janout V, Holcatova I, Foretova L, Brisuda A, Lesueur F, McKay J, Brennan P and Scelo G. Integrative genome-wide gene expression profiling of clear cell renal cell carcinoma in Czech Republic and in the United States. PLoS One 2013; 8: e57886.
[27] von Roemeling CA, Radisky DC, Marlow LA, Cooper SJ, Grebe SK, Anastasiadis PZ, Tun HW and Copland JA. Neuronal Pentraxin 2 supports clear cell renal cell carcinoma by activating the AMPA-selective glutamate receptor-4. Cancer Res 2014; 74: 4796-4810.
[28] Jones J, Otu H, Spentzos D, Kolia S, Inan M, Beecken WD, Fellbaum C, Gu X, Joseph M, Pantuck AJ, Jonas D and Libermann TA. Gene signatures of progression and metastasis in renal cell cancer. Clin Cancer Res 2005; 11: 5730-5739.
[29] Newman AM, Liu CL, Green MR, Gentles AJ, Feng W, Xu Y, Hoang CD, Diehn M and Alizadeh AA. Robust enumeration of cell subsets from tissue expression profiles. Nat Methods 2015; 12: 453-457.
[30] Chandrashekar DS, Karthikeyan SK, Korla PK, Patel H, Shovon AR, Athar M, Netto GJ, Qin ZS, Kumar S, Manne U, Creighton CJ and Varambally S. UALCAN: an update to the integrated cancer data analysis platform. Neoplasia 2022; 25: 18-27.
[31] Feng C, Song C, Liu Y, Qian F, Gao Y, Ning Z, Wang Q, Jiang Y, Li Y, Li M, Chen J, Zhang J and Li C. KnockTF: a comprehensive human gene expression profile database with knockdown/knockout of transcription factors. Nucleic Acids Res 2020; 48: D93-D100.
[32] ENCODE Project Consortium. An integrated encyclopedia of DNA elements in the human genome. Nature 2012; 489: 57-74.
[33] Zhang Q, Liu W, Zhang HM, Xie GY, Miao YR, Xia M and Guo AY. hTFtarget: a comprehensive database for regulations of human transcription factors and their targets. Genomics Proteomics Bioinformatics 2020; 18: 120-128.
[34] Yevshin I, Sharipov R, Kolmykov S, Kondrakhin Y and Kolpakov F. GTRD: a database on gene transcription regulation-2019 update. Nucleic Acids Res 2019; 47: D100-D105.
[35] Zou Z, Ohta T and Oki S. ChIP-Atlas 3.0: a data-mining suite to explore chromosome architecture together with large-scale regulome data. Nucleic Acids Res 2024; 52: W45-W53.
[36] Rauluseviciute I, Riudavets-Puig R, Blanc-Mathieu R, Castro-Mondragon JA, Ferenc K, Ku-

mar V, Lemma RB, Lucas J, Chèneby J, Baranasic D, Khan A, Fornes O, Gundersen S, Johansen M, Hovig E, Lenhard B, Sandelin A, Wasserman WW, Parcy F and Mathelier A. JASPAR 2024: 20th anniversary of the open-access database of transcription factor binding profiles. Nucleic Acids Res 2024; 52: D174-D182.

[37] Rose TL and Kim WY. Renal cell carcinoma: a review. JAMA 2024; 332: 1001-1010.

[38] Ma D, Liu P, Wang P, Zhou Z, Fang Q and Wang J. PKC-beta/Alox5 axis activation promotes Bcr-Abl-independent TKI-resistance in chronic myeloid leukemia. J Cell Physiol 2021; 236: 6312-6327.

[39] Wang D, Li Y, Zhang C, Li X and Yu J. MiR-216a-3p inhibits colorectal cancer cell proliferation through direct targeting COX-2 and ALOX5. J Cell Biochem 2018; 119: 1755-1766.

[40] Ning H, Jiang Y, Li B, Ren J, Wang C, Wei L, Li L, Ran A, Li Z, Li J, Li W, Wang Y and Xiao B. CircABCA1 promotes ccRCC by reprogramming cholesterol metabolism and facilitating M2 macrophage polarization through IGF2BP3-mediated stabilization of SCARB1 mRNA. Mol Cancer 2025; 24: 199.

[41] Ge Q, Meng J, Wang Z, Anwaier A, Lu J, Tian X, Wang Y, Yang J, Zhang H, Ye D and Xu W. Spatially segregated APOE(+) macrophages restrict immunotherapy efficacy in clear cell renal cell carcinoma. Theranostics 2025; 15: 5312-5336.

[42] Kzhyshkowska J, Shen J and Larionova I. Targeting of TAMs: can we be more clever than cancer cells? Cell Mol Immunol 2024; 21: 1376-1409.

[43] Yang L, Shao Y, Zhang Z, Li Y, Wang F and Yu H. Metabolic insights into TAMs and the tumor immune microenvironment: regulatory mechanisms and therapeutic interventions. Biochim Biophys Acta Rev Cancer 2025; 1880: 189411.

[44] García García A, Ferrer Aporta M, Vallejo Palma G, Giráldez Trujillo A, Castillo-González R, Calzón Lozano D, Mora Perdiguero A, Muñoz Velasco R, Colina Castro M, de Simone Benito E, Torres-Ruiz R, Rodriguez-Perales S, Dehairs J, Swinnen JV, Garcia-Cañaveras JC, Lahoz A, Montalvo Quirós S, Del Pozo-Rojas C, Luque Rioja C, Monroy F, Herráez-Aguilar D, Alonso Riaño M, Rodríguez Peralto JL and Sánchez-Arévalo Lobo VJ. Targeting ELOVL6 to disrupt c-MYC driven lipid metabolism in pancreatic cancer enhances chemosensitivity. Nat Commun 2025; 16: 1694.

[45] Fatma H, Maurya SK and Siddique HR. Epigenetic modifications of c-MYC: role in cancer cell reprogramming, progression and chemoresistance. Semin Cancer Biol 2022; 83: 166-176.

Supplementary Materials

Clinical specimens

Primary clear cell renal cell carcinoma (ccRCC) tissue samples and paired adjacent non-tumorous renal tissues were collected from patients undergoing nephrectomy at the Department of Urology, Tongji Hospital (Shanghai, China) between July 2023 and May 2024. All diagnoses were confirmed by board-certified pathologists. The retrospective use of these archived specimens was approved by the Ethics Committee of Tongji Hospital (Approval No. K-2026-077), and written informed consent was obtained from all participants. Tissue samples were snap-frozen in liquid nitrogen and stored at -80°C for further experiments.

Cell lines and culture conditions

The human ccRCC cell lines 786-O, 769-P, Caki-1, and OSRC-2; the normal renal tubular epithelial cell line HK-2; and the human monocytic cell line THP-1 were obtained from the Cell Bank of the Chinese Academy of Sciences (Shanghai, China). Cells were maintained in their recommended culture media (RPMI-1640 or DMEM for ccRCC and HK-2 cells; RPMI-1640 for THP-1), supplemented with 10% fetal bovine serum and 1% penicillin-streptomycin, at 37°C in a humidified incubator with 5% CO_2. For co-culture experiments, THP-1 monocytes were differentiated using 100 nM PMA for 24 h. All cell lines were authenticated by short tandem repeat (STR) profiling and routinely verified to be mycoplasma-free.

Cell infection and transfection

Lentiviral particles carrying shRNA targeting ALOX5 (Sangon Biotech, Shanghai, China) or c-Myc (GeneChem, Shanghai, China) were used to infect 769-P and 786-O cells with polybrene (8 μg/mL) for 24 hours. Following viral transduction, the culture medium was refreshed, and cells underwent puromycin selection at a concentration of 1-2 μg/mL over a five- to seven-day period. This antibiotic treatment protocol enabled the establishment of stable knockdown cell lines targeting ALOX5 and c-Myc genes (designated sh-ALOX5 and sh-c-Myc), alongside their matching negative control counterparts (sh-NC). qRT-PCR and Western blot analyses confirmed effective gene silencing. For overexpression experiments, plasmids encoding ALOX5 were obtained from HANBIO (Shanghai, China) and verified by DNA sequencing. Transient transfections were performed using Lipofectamine 3000 when cells reached approximately 70% confluence. Cells were harvested 36-48 h after transfection for subsequent analyses. The sequences of the shRNAs used in this study are provided in Table S1.

Quantitative real-time PCR (qRT-PCR)

RNA from different cell samples was isolated using TRIzol Reagent (Invitrogen), and its corresponding cDNA was synthesized with the PrimeScript RT Reagent Kit (Takara). Quantitative PCR was performed on an ABI 7500 system (SYBR Green Master Mix, Takara). Gene expression was quantified using the $2^{(-\Delta\Delta Ct)}$ method, normalizing to β-actin. Primer sequences are listed in Table S2.

Western blot analysis

Total protein was extracted using RIPA buffer, and concentrations were determined with the BCA Protein Assay Kit (Thermo Scientific). Proteins were separated by 10% SDS-PAGE and transferred to PVDF membranes. After blocking for 90 minutes, membranes were incubated overnight with primary antibodies at 4°C, followed by 1-hour incubation with HRP-conjugated secondary antibodies. Bands were visualized using an ECL system. Antibody details are provided in Table S3.

Cell proliferation assay

Cell proliferation was assessed using the CCK-8 assay (Beyotime) according to the manufacturer's instructions. Briefly, cells were seeded in 96-well plates (3×10^3 cells/well). At 12-hour intervals for up

to 72 hours, 10 μL of CCK-8 solution was added, and absorbance at 450 nm was measured after 1-hour incubation in the dark.

Migration and invasion assays

Cell migration and invasion were assessed using Transwell inserts (Corning). Cells suspended in serum-free medium were seeded into the upper chambers, with the lower compartments containing medium supplemented with 10% FBS as a chemoattractant. For invasion assays, inserts were pre-coated with Matrigel. Cells on the membrane's underside were fixed, stained with crystal violet, and counted in five randomly selected fields.

Immunohistochemistry (IHC)

Paraffin-embedded tumor sections (fixed in 4% formaldehyde) were subjected to immunohistochemical staining. After overnight incubation with primary antibodies at 4°C, sections were incubated with corresponding secondary antibodies and streptavidin-HRP. Following hematoxylin counterstaining, images were captured and analyzed using an Olympus BX53 microscope. IHC staining was quantified using the H-score, calculated by multiplying the percentage of positively stained cells by the staining intensity (0-3). The final H-score ranged from 0 to 300, with higher scores indicating stronger protein expression.

Chromatin immunoprecipitation (ChIP) and dual-luciferase reporter assay

Chromatin immunoprecipitation (ChIP) assays were performed using the EZ-ChIP Kit (Millipore) following the manufacturer's protocol. Briefly, ccRCC cells at 90% confluence were cross-linked with 1% formaldehyde for 10 minutes and quenched with 1× glycine. Chromatin was sonicated to 500-1000 bp fragments and immunoprecipitated with anti-c-Myc antibody or normal rabbit IgG. After reverse cross-linking, the purified DNA was analyzed by qRT-PCR to assess c-Myc binding at the ALOX5 promoter region.

For the dual-luciferase reporter assay, 769-P, 786-0, and HEK293T cells were co-transfected with a firefly luciferase construct driven by either the wild-type or mutant ALOX5 promoter (c-Myc binding site mutated), along with a Renilla luciferase plasmid for normalization. Where indicated, a c-Myc expression plasmid or empty vector was co-transfected. Luciferase activity was measured 48 hours post-transfection, and relative transcriptional activation of the ALOX5 promoter by c-Myc was calculated.

Immunofluorescence (IF)

The samples were washed 3 times with PBS and fixed with 4% paraformaldehyde for 10 minutes at room temperature. Nonspecific binding was blocked by incubation with 5% BSA for 30 minutes at 37°C. The samples were then incubated overnight at 4°C with anti-CD206 primary antibody, followed by a 1-hour incubation at room temperature with a species-matched fluorescent secondary antibody. Nucleus were marked with DAPI for 5 minutes. Fluorescence was visualized using an Olympus fluorescence microscope. Typical images were taken followed by intensity quantification using ImageJ software.

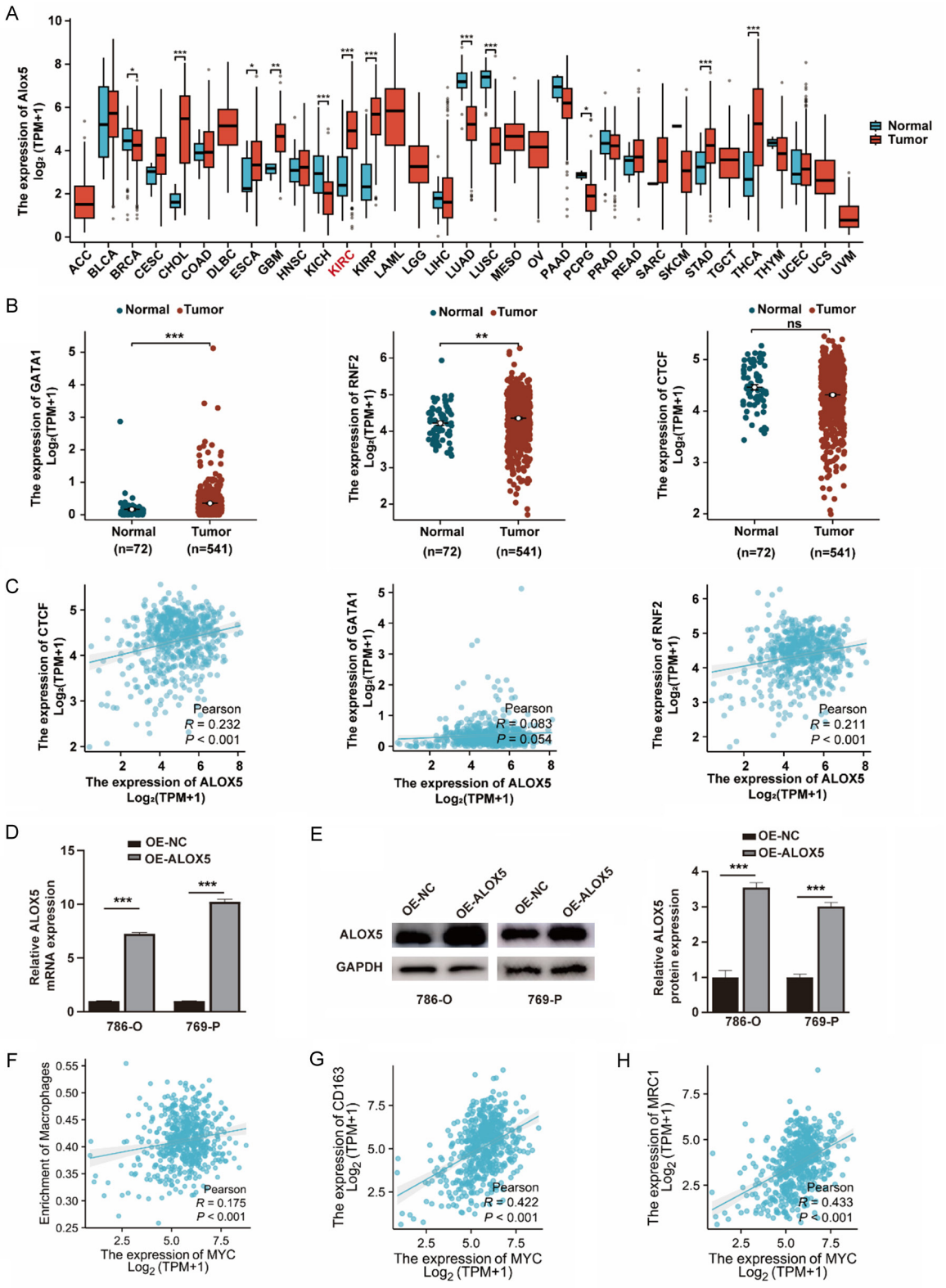

Figure S1. A. Pan-cancer differential expression analysis of ALOX5 in the TCGA-KIRC database. B. Differential expression analysis of three transcription factors (GATA1, RNF2, and CTCF) in the TCGA-KIRC database. C. Correlation analysis between GATA1, RNF2, and CTCF expression and ALOX5 levels in the TCGA-KIRC dataset. D, E. Validation of increased ALOX5 mRNA and protein expression levels in ALOX5-overexpressing cells by qRT-PCR and Western blot analyses. F. Correlation analysis between c-Myc expression and macrophage infiltration levels. G. Correlation

analysis between c-Myc expression and M2 macrophage marker (CD163) in the TCGA-KIRC dataset. H. Correlation analysis between c-Myc expression and the M2 macrophage marker MRC1 (CD206) in the TCGA-KIRC dataset. *P < 0.05, **P < 0.01, ***P < 0.001.

Table S1. Sequences of shRNAs used in this study

shRNA ID	shRNA Sequence (5'→3')
sh-ALOX5-1#	CGGGAGATGAGAACCCTATTT
sh-ALOX5-2#	CGAGATGACCAAATTCACATT
sh-ALOX5-3#	CCCGTGATATCCAGTTTGATA
sh-c-Myc-1#	CCATAATGTAAACTGCCTCAA
sh-c-Myc-2#	CAGTTGAAACACAAACTTGAA
sh-c-Myc-3#	CCTGAGACAGATCAGCAACAA

Table S2. Primer sequences used for qRT-PCR

Gene	Primer
β-actin	F: CATGTACGTTGCTATCCAGGC | R: CTCCTTAATGTCACGCACGAT
ALOX5	F: ACAAGCCCTTCTACAACGACT | R: AGCTGGATCTCGCCCAGTT
c-Myc	F: GGCTCCTGGCAAAAGGTCA | R: CTGCGTAGTTGTGCTGATGT
CD163	F: TTTGTCAACTTGAGTCCCTTCAC | R: TCCCGCTACACTTGTTTTCAC
CD206	F: TCCGGGTGCTGTTCTCCTA | R: CCAGTCTGTTTTTGATGGCACT
Arg-1	F: GTGGAAACTTGCATGGACAAC | R: AATCCTGGCACATCGGGAATC
IL-10	F: GACTTTAAGGGTTACCTGGGTTG | R: TCACATGCGCCTTGATGTCTG
E-cadherin	F: CGAGAGCTACACGTTCACGG | R: GGGTGTCGAGGGAAAAATAGG
N-cadherin	F: TCAGGCGTCTGTAGAGGCTT | R: ATGCACATCCTTCGATAAGACTG
Vimentin	F: GACGCCATCAACACCGAGTT | R: CTTTGTCGTTGGTTAGCTGGT

Table S3. Antibodies used in this study

Antibody name	Manufacturer	Article Number
ALOX5	Proteintech	83794-4-RR
C-Myc	Proteintech	10828-1-AP
GAPDH	Proteintech	60004-1-Ig
E-cadherin	Proteintech	20874-1-AP
N-cadherin	HUABIO	SY02-46
Vimentin	Proteintech	10366-1-AP
ARG-1	Proteintech	16001-1-AP
CD206	Proteintech	18704-1-AP
secondary antibodies	proteintech	RGAR001

Table S4. Association between ALOX5 expression and clinicopathological characteristics in the TCGA-KIRC cohort

Characteristics	Low expression of ALOX5	High expression of ALOX5	*p* value	statistic	method
N	270	271			
Pathologic T stage, n (%)			0.3	3.67	Chisq test
T1	144 (26.6%)	135 (25%)			
T2	40 (7.4%)	31 (5.7%)			
T3	82 (15.2%)	98 (18.1%)			
T4	4 (0.7%)	7 (1.3%)			
Pathologic N stage, n (%)			0.03	4.7	Chisq test
N0	113 (43.8%)	129 (50%)			
N1	3 (1.2%)	13 (5%)			
Pathologic M stage, n (%)			0.04	4.17	Chisq test
M0	222 (43.7%)	207 (40.7%)			
M1	31 (6.1%)	48 (9.4%)			
Pathologic stage, n (%)			0.22	4.36	Chisq test
Stage I	143 (26.6%)	130 (24.2%)			
Stage II	33 (6.1%)	26 (4.8%)			
Stage III	59 (11%)	64 (11.9%)			
Stage IV	34 (6.3%)	49 (9.1%)			
Gender, n (%)			0.31	1.05	Chisq test
Female	99 (18.3%)	88 (16.3%)			
Male	171 (31.6%)	183 (33.8%)			
Age, n (%)			0.21	1.56	Chisq test
≤ 60	127 (23.5%)	142 (26.2%)			
> 60	143 (26.4%)	129 (23.8%)			
Histologic grade, n (%)			0.26	4.04	Chisq test
G1	8 (1.5%)	6 (1.1%)			
G2	123 (23.1%)	113 (21.2%)			
G3	103 (19.3%)	104 (19.5%)			
G4	30 (5.6%)	46 (8.6%)			
Laterality, n (%)			0.26	1.26	Chisq test
Left	120 (22.2%)	133 (24.6%)			
Right	150 (27.8%)	137 (25.4%)			
Therapy outcome (%)			0.17	5	Yates' correction
PD	7 (4.8%)	4 (2.7%)			
SD	5 (3.4%)	1 (0.7%)			
PR	0 (0%)	2 (1.4%)			
CR	67 (45.6%)	61 (41.5%)			